Morphology Development for Single-Site Ethylene Copolymers in Rotational Molding

H. Xu, C. T. Bellehumeur

Schulich School of Engineering, Department of Chemical and Petroleum Engineering, University of Calgary, Calgary, AB, Canada T2N 1N4

ABSTRACT: The morphology development of ethylene copolymers was modeled with the modified phase-field theory. The metastability of polymer crystallization was also considered in the modeling. Modeling and experimental work were simultaneously undertaken to compare the crystallization kinetics of single-site-catalyzed and Ziegler-catalyzed resins and their influence on morphology development in the rotational-molding process. With a more uniform short-chain branch distribution, the single-site copolymers developed well-defined spherulitic structures. The Ziegler–Natta catalyst resins were characterized by a higher nuclei density and a faster crystallization rate and produced finer structures in the molded parts. The modeling approach proposed in our work allowed an evaluation of the processing and the material effects on the development of morphological features during melt solidification. © 2007 Wiley Periodicals, Inc. J Appl Polym Sci 107: 236–245, 2008

Key words: crystallization; modeling; molding; morphology; polyethylene (PE); processing; simulations

INTRODUCTION

Over the last decade, polyolefins based on metallocene and single-site-catalyst technologies have been finding increasing use in many applications. These technologies allow for better control of the molecular structure, that is, the molecular weight distribution and chemical composition. Variations in the molecular characteristics of polyolefins can have an important impact on the processing behavior of materials and on the physical, chemical, and mechanical performance of molded parts. Although single-site-catalyst polymers have been the subject of many studies, few studies have evaluated them for rotational-molding applications. Although the potential use of single-site polyolefins in rotational-molding applications has been investigated,[1–6] early publications focused mostly on the perceived processing advantage of metallocene resins over Ziegler-catalyzed resins. Attention is paid to the solidification stage in this article because it dictates the final morphology of the material and the properties of the end product.

The objective of this work is to compare and model the morphology development of single-site-catalyzed and Ziegler-catalyzed resins in rotational molding. The morphology development of ethylene copolymers in the rotational-molding process has been reported in a separate publication.[7] In this study, we consider single-site polyethylene copolymers with a tailored molecular structure and composition but with attributes otherwise comparable to commercial Ziegler–Natta rotomolding-grade resins. A two-dimensional theoretical simulation is carried out, consisting of a phase-field model emphasizing the metastability of polymer crystallization and a heat-transfer model describing the molding cycle. The model is used to evaluate the morphological structure across the molded part, and predictions are validated with results obtained from molding trials. Although the dependence of semicrystalline polymers on their microstructure is widely accepted, the establishment of useful relationships is not a simple task. The proposed modeling approach is a departure from approaches traditionally considered in polymer processing and represents an important milestone in the development of structure–processing property relationships in rotational molding.

EXPERIMENTAL

Materials

Five rotational-molding-grade ethylene copolymers were selected to carry out molding experiments. Among them were three commercial hexene–ethylene copolymers (Novapol TR-0535, Novapol TR-0338, and Novapol TR-0242) and two single-site-catalyst

TABLE I
Material Properties

Resin	Type	MFI (g/10 min)[a]	Density (g/cm^3)[b]	M_w (g/mol)	M_w/M_n	CDBI
ZN535	Ethylene–hexene copolymer	5.0	0.935	69,300	3.55	29
ZN338	Ethylene–hexene copolymer	3.5	0.938	77,000	2.95	45
ZN242	Ethylene–hexene copolymer	1.8	0.942	90,600	3.47	51
S539	Ethylene–octene copolymer	5.2	0.939	65,500	2.26	74
S244	Ethylene–octene copolymer	1.7	0.944	91,600	2.65	75

MFI = melt flow index; M_n = number-average molecular weight; M_w = weight-average molecular weight.
[a] At 190°C (ASTM D 1238).
[b] According to ASTM 792.

octene–ethylene copolymers. The resins are called ZN535, ZN338, ZN242, S539, and S244, respectively; the prefixes indicate the catalyst technology used in the synthesis of the polymer: ZN for Ziegler–Natta and S for single-site. Molecular weight distributions were determined by high-temperature gel permeation chromatography with a Waters 150C (Mississauga, Ontario, Canada) high-temperature gel permeation chromatograph with a differential refractive-index detector in accordance with ASTM D 6474. Temperature rising elution fractionation (analytical) tests were also performed with a slurry pack technique. The specimens were dissolved in 1,2,4-trichlorobenzene (TCB) at 150°C. Crystallization was carried out from 110 to 0°C at 0.025°C/min. A slurry was obtained through the addition of acetone and Celite-545 and was then packed into a stainless steel column. Elution was carried out with TCB (2 mL/min from 24.5 to 110°C at 0.25°C/min), and the concentration of the eluted solution was monitored with an IR detector cell. The comonomer distribution broadness index (CDBI) was determined on the basis of the temperature rising elution fractionation results and is defined as the percentage of polymers with compositions within 50% of the median comonomer composition,[8] low values being indicative of broader comonomer distributions. The molecular characteristics and key material properties of all the resins considered in this work are presented in Table I.

Molding

Molding trials were conducted on a bench-scale uniaxial rotational-molding machine. The oven cavity was about 38.5 cm long and had an inner diameter of 30 cm. The heating of the oven cavity was performed with two electrical semicircular heating panels. Two fans were placed in the front of the oven to ensure proper air circulation and a uniform temperature distribution. Thermocouples were in position to monitor the oven temperature and the air temperature inside the mold. The measurements were recorded and analyzed with an analog–digital con-

verter data acquisition card (6024E) and Labview 6/7 software (National Instruments, Austin, TX).

All resins were received in a powder form and molded to generate parts with an average thickness of 5 mm with an aluminum box mold (8 × 8 × 15 cm^3 for the inner cavity). The mold rotation speed was set to 6 rpm, and the oven temperature was kept constant throughout the heating cycle (270°C). The heating time was varied to achieve an inside air temperature of 190 ± 2°C. The air temperature inside the mold was monitored and used to control the molding cycle. During the cooling stage of the molding process, the mold remained in rotation while being subjected to two different cooling conditions: still air and water spray (single water spray).

Measurements

The melting and crystallization of the polymers were studied with differential scanning calorimetry (DSC) and hot-stage microscopy techniques. Variations in the equilibrium melting temperature (T_m^0), with changes in the molecular structure, were taken into consideration in this work. T_m^0 was determined experimentally from isothermal crystallization tests conducted on a TA Instruments (New Castle, DE) Q100 differential scanning calorimeter. The specimens weighed in the range of 5–10 mg, and during the DSC measurements, dried N_2 gas was purged at a constant flow rate. The specimens were first heated at 10°C/min to 200°C and maintained at that temperature for 10 min. The specimens were then cooled at a rate of 10°C/min to 0°C for a nonisothermal crystallization behavior study. For isothermal crystallization experiments, the specimens were quenched from the melt to a predetermined crystallization temperature at a rate of 100°C/min and held at that temperature until the crystallization was completed. Thereafter, the specimens were heated again to obtain the DSC endotherms at a rate of 10°C/min. The equilibrium melting point of the resins was obtained through a Hoffman–Weeks plot.[9]

Measurements of the spherulite growth rate were performed with a Mettler–Toledo (Columbus, OH)

FP82 hot stage coupled with an Olympus (Center Valley, PA) B201 optical microscope. To ensure better temperature control and avoid thermal oxidation, the hot stage was cooled with nitrogen gas. Specimens 20 μm thick were prepared with a Leica (Wetzlar, Germany) RM2165 microtome. The films were heated between glass slides and cover slips at the hot stage to 200°C for 30 min before rapid cooling to the isothermal crystallization temperature. The crystallization of the specimens was captured with an Olympus B201 optical microscope coupled to a charged coupling device video recorder connected to a computer, which recorded the data.

The superstructure that formed during the solidification process was characterized from microphotographs of cross sections of the molded parts. Thin layers along the cross sections (20 μm) of the molded parts were cut with a Leica RM2165 microtome. The specimens were viewed under polarized light optical microscopy, and pictures were taken in areas close to each edge (mold and free surface).

THEORETICAL MODELING

In the rotational-molding process, the powder gradually adheres to and melts onto the mold without forced pressure; thus, negligible flow deformation occurs within the materials. As cooling proceeds, the crystallization rate is highly dependent on the temperature. The heat transfer during the cooling stage of the process is primarily ensured by forced convection at the mold surface. The crystallization front moves from the outer surface toward the inner surface of the polymer layer. The cooling is relatively slow compared with that seen in other processes, and as a result, large spherulites are produced in the semicrystalline polymer parts. Several studies have been devoted to developing models describing heat transfer in the rotational-molding process. Initially, Throne[10] established a simple approximate model to investigate various effects on cooling rates without addressing the crystallization process. Subsequently, polymer crystallization during rotational molding has been modeled with the moving interface method[11,12] or Stefan problem, which has been proven very useful in metallic materials; however, it is not suitable for polymeric materials because the latter are characterized by an interval of temperatures in which a melt–solid transition occurs. To better represent the nature of the phase transitions in polymers, a different kind of approach has been applied for crystallization simulation during rotational molding. It considers the latent heat in the transition interval in the heat-transfer process, and the crystallization parameters are determined through DSC.[13,14] Furthermore, Martins et al.[15] evaluated the relationship between the spherulite growth rate data and half of

the crystallization time, took the average nuclei density of isothermally crystallized polypropylene as a function of the crystallization temperature, and predicted the spherulite size in rotationally molded polypropylene by extending it to nonisothermal crystallization conditions.

Avrami's work and the Lauritzen–Hoffman nucleation theory have served as the basis of numerous studies carried out to model polymer crystallization. As the most tested kinetic theories, both focus on the physical essentials of polymer crystallization and are thus limited to considering temporal development and lack spatial diffusion of the interface. To predict the spatiotemporal crystal growth and describe the evolution of the crystal shape in two or three dimensions, we propose the use of the modified phase-field theory to elucidate the solidification phenomena in semicrystalline polymers.[16–18] The phase-field model treats the sharp interfaces as spatially diffuse interfaces of finite thickness through the expression of order parameters; a typical phase-field profile across the interface resembles the form of a solitary wave. This distinguishes between phases undergoing solidification.[19–23] The advantage of this treatment over other diffusional growth (Laplacian) models is that there is no need to track the interface, and the whole domain is treated in the same way numerically. Various phase-field models have been successfully applied to material processes.[21,22,24,25] The one used in this study has been extended to describe the solidification of high-molecular-weight polymers with the incorporation of metastability, the free-energy density being supercooling-dependent.[16–18]

Heat-transfer model

The thermal analysis of the process followed that described by Xu and Bellehumeur.[7] During the heating stage of the molding cycle, the powder was assumed to be well mixed. The curvature effects were also assumed to be negligible. For the heat conduction through the polymer material, the energy equation considered the impact of latent heat, which manifested as positive values as a function of the degree of melting (X_m) during melting and as negative values related to the degree of crystallization (X_c) during crystallization:

$$\frac{\partial}{\partial z}\left(k\frac{\partial T}{\partial z}\right) = \frac{d}{dt}(\rho C_p T) + \rho H_m \frac{dX_m}{dt} \quad \text{(when heating)}$$

(1)

$$\frac{\partial}{\partial z}\left(k\frac{\partial T}{\partial z}\right) = \frac{d}{dt}(\rho C_p T) - \rho H_c \frac{dX_c}{dt} \quad \text{(when cooling)}$$

(2)

where k is the thermal conductivity of the polymers, ρ is the density of the polymer system, and C_p is the

specific heat capacity. Also, the terms H_m and H_c represent the total latent heat related to the phase transition, and the degree of transition is defined as the ratio of the mass that has already undergone a transition at time t to the total mass. The values for these parameters were obtained through DSC measurements.

The different boundary conditions at the interface of the regions were characterized by different material properties as follows:

$$-k_s \frac{\partial T}{\partial z}\Big|_{os} = h_o(T_o - T_{os}) \quad \text{(at the mold outer surface)} \tag{3}$$

$$-k_s \frac{\partial T}{\partial z}\Big|_{sp} = -k_p \frac{\partial T}{\partial z}\Big|_{ps} \quad \text{(at the mold}-\text{polymer interface)} \tag{4}$$

$$h_a(T_{pa} - T_a) = -k_p \frac{\partial T}{\partial z}\Big|_{pa} \quad \text{(at the polymer}-\text{air interface)} \tag{5}$$

During the cooling progress, eq. (3) can be written as follows:

$$-k_s \frac{\partial T_s}{\partial z}\Big|_{os} = h_{sa}(T_o - T_{os}) \quad \text{(still}-\text{air cooling)} \tag{3a}$$

$$-k_s \frac{\partial T_s}{\partial z}\Big|_{os} = h_{ws}(T_o - T_{os}) \quad \text{(water}-\text{spray cooling)} \tag{3b}$$

where k_s is the thermal conductivity of the mold; T_s is the mold temperature; T_o is the oven temperature; h_o, h_{sa}, and h_{ws} represent the convective coefficients of heating, still-air cooling, and water-spray cooling, respectively; T_{os} is the temperature at the mold outer surface; and h_a and T_{pa} indicate the convective coefficient and temperature at the polymer–air interface, respectively. The subscripts s, o, p, and a indicate the mold, oven, polymer, and internal air, respectively. In the simulation, the initial conditions are the mold, polymer, and air at room temperature (25°C).

Phase-field model

A phase-field model including consideration of the metastability of polymer crystallization was used to describe spatiotemporal morphology development during the cooling process in rotational molding. In phase-field modeling, the Ginzburg–Landau free energy[19–23] is defined for a pure material to treat the system as a whole. The total free energy [$F(\psi)$] of the nonconserved crystal ordering involves a local free-energy density and a nonlocal gradient term, which represent nucleation and growth separately:

$$F(\psi) = \int [f_{\text{local}}(\psi, T) + f_{\text{grad}}(\psi, T)] d\Omega \tag{6}$$

where

$$f_{\text{local}}(\psi, T) = \left[\frac{\zeta \psi_0}{2} \psi^2 - \frac{\zeta + \psi_0}{3} \psi^3 + \frac{\psi^4}{4} \right] \tag{7}$$

$$f_{\text{grad}}(\psi) = \frac{1}{2} (\kappa \cdot \nabla \psi)^2 \tag{8}$$

Ω is the integration field, and κ is the gradient coefficient. ψ represents the crystal order parameter at time t and position r, describing the extent of structural change during crystallization.

For the polymer material, the crystal melting temperature obtained at a given crystallization condition is always different from that of the equilibrium melting point. Therefore, the various metastable crystal states in polymer solidifications reveal various hierarchy morphologies ranging from disordered spherulites to highly ordered single crystals. This introduces the term ψ_0, which is defined as the ratio of the melting temperature to the equilibrium melting point. ψ_0 is proposed to describe the minimum free energy representing the metastable solid crystal, which is a function of supercooling according to the Hoffman–Weeks relationship.[9] The local free-energy density of the system in eq. (7) is proposed to be a monotonic function of temperature $T(r,t)$ and has the form of an asymmetric double well with respect to ψ. ζ represents the value of order parameter ψ at the nucleation barrier peak, whereas W is a dimensionless coefficient describing the height of the energy barrier for nucleation. Both ζ and W are related to the supercooling.

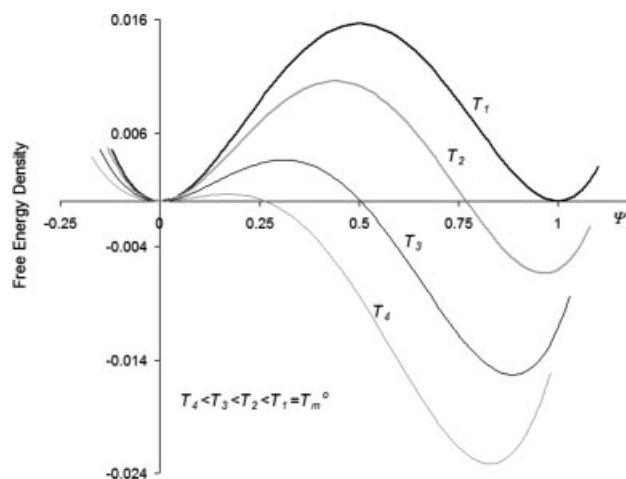As shown in Figure 1, as the temperature increases, the crystal state can be varied from some

Figure 1 Variation of the local free-energy density as a function of crystal order parameter ψ for various temperatures, showing different nucleation barrier heights and locations (ζ). The crystal state, $\psi = \psi_0$, varies with the crystallization temperature, indicating the imperfection of the polymer crystals.

finite values of ψ_0 to unity at equilibrium, thereby capturing various metastable states. At a deep supercooling, ψ_0 shifts to the left to become significantly lower than 1, and this means that the final obtained crystal contains more defects.[16,17] The uniqueness of the proposed approach is that there is no need for considering the multiple metastable wells to account for the metastability potentials of polymer crystallization. A simple free-energy double well with various (supercooling-dependent) ψ_0 values would serve the same purpose without losing the physical essence of the general solidification. The gradient contribution is included in eq. (8) to describe the growth process, leading to a diffuse crystal–liquid interface. κ depends on the crystal–melt interface property.

As usual in the practice of phase-field modeling, the microstructure development was characterized by the spatiotemporal evolution of the order parameter, and the Langevin noise term (η_ψ) was added to model thermal fluctuations. Essentially, the governed time-dependent Ginzburg–Landau theory or model A equation can be expressed as follows:

$$\frac{\partial \psi(r, t)}{\partial t} = -\Gamma \frac{\delta F(\psi)}{\delta \psi}$$
$$= -\Gamma \left[W\psi(\psi - \zeta)(\psi - \psi_0) - \kappa^2 \nabla^2 \psi \right] + \eta_\psi \quad (9)$$

where Γ is the mobility. η_ψ has a zero mean, and the amplitudes are given by the fluctuation–dissipation theorem:[26,27]

$$<\eta(r, t)\eta(r', t')> = 2k_B T \Gamma \delta(r - r')\delta(t - t') \quad (10)$$

where k_B is the Boltzmann constant and $\delta(r - r')$ and $\delta(t - t')$ are Dirac delta functions.

It is well known that the temperature plays a significant role in the crystallization process. The temperature distribution during the cooling stage can be determined with a modified heat-transfer equation:

$$\frac{\partial}{\partial z}\left(k\frac{\partial T}{\partial z}\right) = \frac{d}{dt}(\rho C_p T) - \rho H_c X_c \frac{d\psi}{dt} \quad (11)$$

NUMERICAL MODEL

Numerical values of the model parameters were either obtained experimentally or estimated from data published in the literature. After the previous article,[7] the variations of physical and thermal properties with the temperature were considered. The temperature dependence of the heat capacity was obtained from DSC measurements for the polymers. The density and thermal conductivity were determined with a simple linear mixing rule for simplicity (m for melt and c for crystal):

$$\rho = X_m \rho_m + (1 - X_m)\rho_{\text{powder}} \quad \text{(heating)} \quad (12)$$

$$\rho = X_c \rho_c + (1 - X_c)\rho_m \quad \text{(cooling)} \quad (13)$$

$$k_p = \frac{\rho}{\rho_c} k_{p\infty} \quad (14)$$

where ρ_{powder} is the density of the powder, ρ_c is the density of the crystal, and ρ_m is the density of the melt. $k_{p\infty}$ is the thermal conductivity of the polymer crystal. No other variation of the thermal properties has been assumed for the mold material.

During rotational molding, the density of nuclei is greatly affected by the cooling conditions, increasing at a lower temperature or a faster cooling rate. The nucleation process is simulated with the introduction of uncorrelated η_ψ terms into the crystallization equation [eq. (9)]. These fluctuations are placed in the field at every time step. As the cooling proceeds, some noises shrink in the melt, whereas other noises increase by overcoming the nucleation energy barrier, which itself is determined by the supercooling. As demonstrated by Allen and Cahn[28] and Wheeler et al.,[22] in the phase-field model, the parameters can be evaluated on the basis of material properties that can be determined experimentally.[7] The numerical values of the parameters are listed in Table II.

The proposed equations were solved numerically with a central finite difference method for spatial discretization and with an explicit forward difference method for time steps with no-flux boundary conditions. Various grid sizes (128 × 128, 256 × 256, and 512 × 512) and temporal steps (Δt) were employed to ascertain the stability of the simulation; however, only the results of the 512 × 512 simulation are presented.

RESULTS AND DISCUSSION

Experimental results

The micrographs obtained with polarized light microscopy reveal that the general crystalline textures of the samples were mainly spherulites with well-defined Maltese crosses and regularly spaced dark bands, which are typical features of polyethylene. Figures 2–6 show the cross-section morphologies obtained for all the resins under different cooling conditions. Although limited temperature measurements were possible, with the help of the simulation, we found that under water-spray cooling, the maximum cooling rate at the mold surface reached 70°C/min, whereas at the free surface, it was only 22°C/min, 2–3 times less than that of the mold surface. The simulated cooling rate profile showed results

TABLE II
Numerical Values of the Parameters Used in the Models

Parameter		Value	Parameter		Value
k_s (W/m K)[a]		147	C_{ps} (J/kg K)[a]		917
$k_{p\infty}$ (W/m K)[b]		0.2	C_{pa} (J/kg K)[b]		1010
ρ_s (kg/m³)[a]		2800	σ (J/m²)[c]		0.0137
ρ_{powder} (kg/m³)[b]		350	h_0 (W/m² K)		12
ρ_m (kg/m³)[b]		900	h_a (W/m² K)[b]		5
ρ_a (kg/m³)[b]		0.95			
Resin	ρ_c (kg/m³)	v (m/s)	H_c (kJ/kg)	H_m (kJ/kg)	T_m^0 (°C)
ZN535	0.935	1.03×10^{-7} (118°C)	143.4	140.8	128.14
ZN338	0.938	1.56×10^{-7} (118°C)	150.0	130.4	127.92
ZN242	0.942	3.92×10^{-7} (118°C)	163.8	144.0	129.56
S539	0.939	6.25×10^{-8} (118°C)	144.2	145.8	124.9
S244	0.944	3.75×10^{-8} (122°C)	165.4	162.3	128.2
Resin	v (m/s)				
ZN535	1×10^{-125} exp[106,127/T (K)]				
ZN338	2×10^{-111} exp[93,501/T (K)]				
ZN242	4×10^{-137} exp[117,128/T (K)]				
S539	1×10^{-137} exp[116,762/T (K)]				
S244	6×10^{-239} exp[209,893/T (K)]				

[a] The data were taken ref. 37.
[b] The data were taken from ref. 14.
[c] The data were taken from ref. 38.

similar to those observed by Martins et al.[15] It is apparent that the cooling rate has a significant impact on the resulting microstructures. All ethylene copolymers show a coarsening and deterioration in the spherulitic structure with decreases in the cooling rate. Under air-cooling conditions, crystallization occurs at higher temperatures, resulting in lower nucleation rates. Because lower cooling rates (air cooling) provide sufficient time for polymer long chains to be incorporated into ordered structures,

they produce bigger spherulite structures, which evolve into stacked lamellae.

Variations in the morphological features across the molded-part thickness are generally expected for rotationally molded products. Our experimental results followed this tendency, variations in the morphological features across the molded-part thickness being more apparent for parts produced under severe cooling conditions (water spray) and with low-density polyethylene resins (ZN535 and S539).
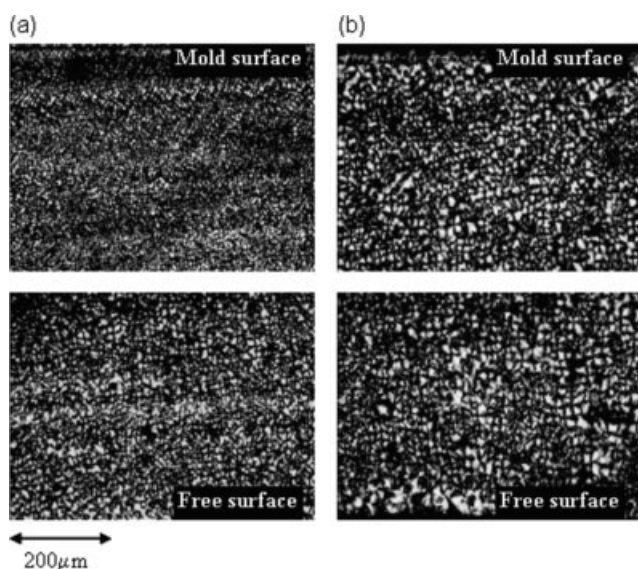

Figure 2 Polarized light microphotographs of a molded-part cross section of ZN535 processed with (a) water-spray and (b) still-air cooling conditions.
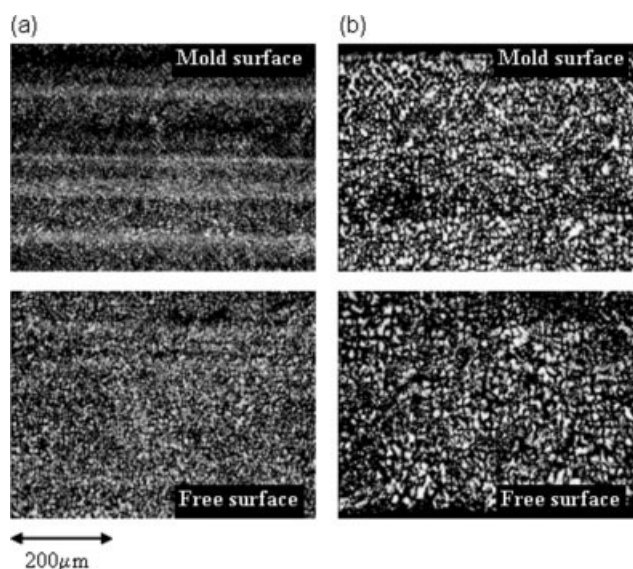

Figure 3 Polarized light microphotographs of a molded-part cross section of ZN338 processed with (a) water-spray and (b) still-air cooling conditions.
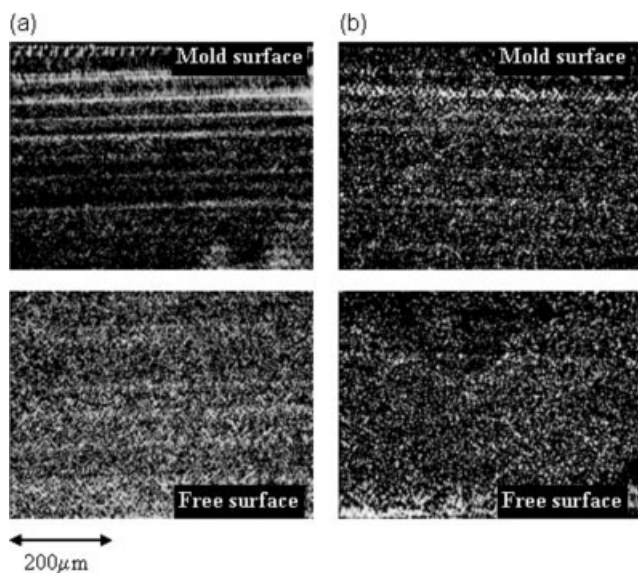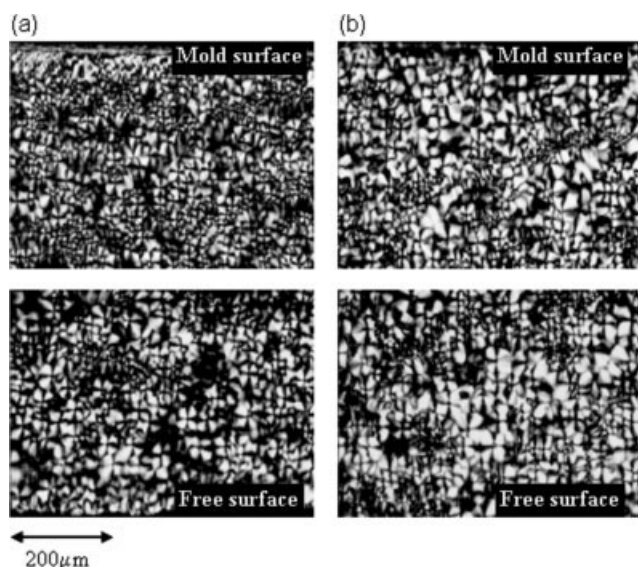
Figure 4 Polarized light microphotographs of a molded-part cross section of ZN242 processed with (a) water-spray and (b) still-air cooling conditions.

Because the regions in close contact with the mold wall cool at a faster rate than the inner surface zone, a large number of heterogeneous nuclei are activated at the polymer–mold interface, experiencing sharper temperature gradients, and they tend to grow parallel to the temperature gradient direction. In addition, the difference in the cooling rates between the mold surface and free surface determines the decrease in the size of the spherulites. The slower cooling rate at the free surface allows for crystallization to occur at higher temperatures and for a longer period, and

this promotes increases in the perfection and size of the crystalline lamellae. Under fast-cooling conditions, the long chains and short side branches will crystallize together, resulting in imperfect or unstable crystals. Under slow cooling, the long-chain segments will crystallize at higher temperatures with stable, perfect crystals, whereas the short branches will not crystallize and will be expelled to the surface of the crystals. At lower temperatures, they tend to create imperfect crystals. Thus, resins with higher comonomer contents respond more severely to a reduction in the cooling rate, and the large number of branching ends relax and assemble themselves into the ordered region, preventing the disruption in the crystal ordering caused by the presence of side branching.

Compared with the Ziegler–Natta-catalyst hexene–ethylene copolymers (ZN535, ZN338, and ZN242), the single-site-catalyst octene–ethylene copolymers (S539 and S244) have narrower molecular weight distributions and a more uniform short-chain branch distribution, as shown by CDBI (Table I). In the conventional Ziegler–Natta catalysts, the multiple active sites polymerize by inserting the comonomer at relatively irregular intervals into the growing ethylene chains, resulting in a broad and heterogeneous branching distribution of branches in polyethylene. In contrast, the single-site catalysts incorporate the comonomer into the ethylene chains rather homogeneously and produce a relatively narrow molecular weight distribution.

The overall branching level influences the resin properties through its control of the crystallinity and morphology. Each branch point and chain end dis-
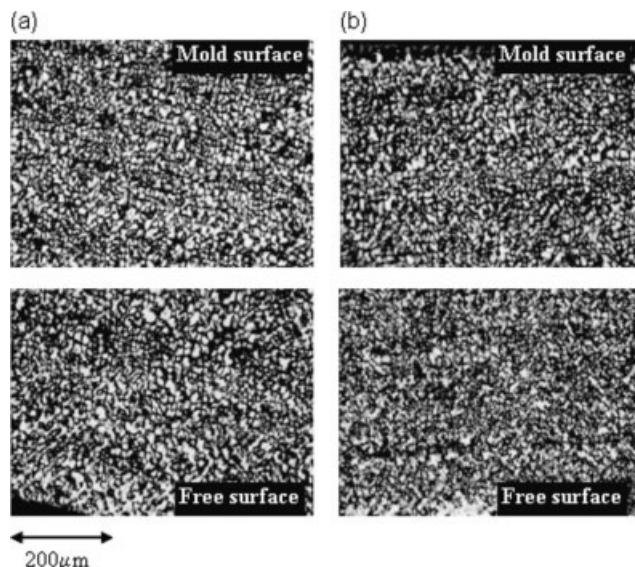

Figure 5 Polarized light microphotographs of a molded-part cross section of S539 processed with (a) water-spray and (b) still-air cooling conditions.

Figure 6 Polarized light microphotographs of a molded-part cross section of S244 processed with (a) water-spray and (b) still-air cooling conditions.

rupts the local order during crystallization and reduces the degree of crystallinity. With higher branch contents in the copolymers, the surface nucleation rate is reduced more than the lateral spreading rate, and it is more difficult for them to form recognizable superstructures. Our microscopic observations obtained with the Ziegler–Natta copolymers (Figs. 2–4) validate the effects of branches on ethylene copolymer morphologies and are in agreement with other previous findings.[29–31] Despite the effect of the cooling conditions, we observed well-developed spherulites with a banded structure for both S539 and S244 (Figs. 5 and 6). On the other hand, the Ziegler–Natta resins, which have comparable or even lower densities, contained spherulites of a much smaller size, which led to finer morphological structures. As shown in Figure 4, parts produced with ZN242 displayed no distinctive superstructure, the cooling rate having the least effect, in this case, on the morphological features and the banding pattern disappearing in optical micrographs.

It has been reported that Ziegler–Natta resins have intermolecular distributions strongly differing from those of single-site resins.[32,33] Typically, the incorporation of comonomer units is higher in lower molar mass chains, generating a fraction of highly defective molecules that do not participate in the crystallization process. The effective comonomer concentration (short-chain branch) is thus lower in the Ziegler–Natta resins than in single-site copolymers of comparable density, and this explains the differences in the nucleation density (Figs. 2–6) and crystal growth velocity observed experimentally (Table II). Any residual catalysts present in the Ziegler–Natta resin matrix would act as heterogeneous nucleating agents. Moreover, the very long chain molecules (absent in
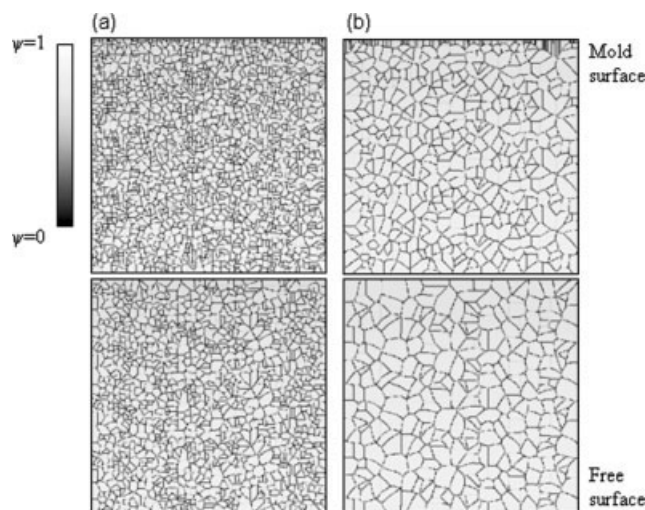

Figure 8 Simulation results showing the morphology of a 5-mm-thick cross section of ZN338 processed with (a) water-spray and (b) still-air cooling conditions.

the single-site resins) may persist in the melt as aggregates and lead to a significant enhancement of the nucleation density. Thus, the nucleating density is expected to be higher for the Ziegler–Natta catalyst copolymers than the single-site resins.

Model predictions

The morphology experimentally observed was simulated with two-dimensional phase-field models with a calculated temperature distribution during the cooling stage. The simulation results for all five resins molded under different cooling conditions are reported in Figures 7–11. We report in these figures
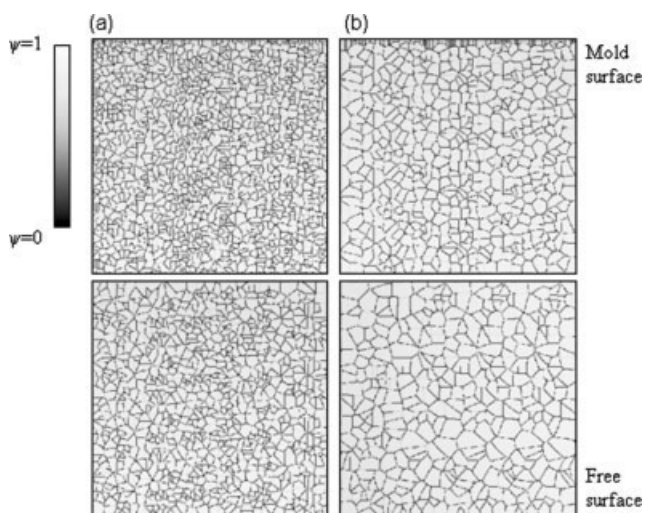

Figure 7 Simulation results showing the morphology of a 5-mm-thick cross section of ZN535 processed with (a) water-spray and (b) still-air cooling conditions.
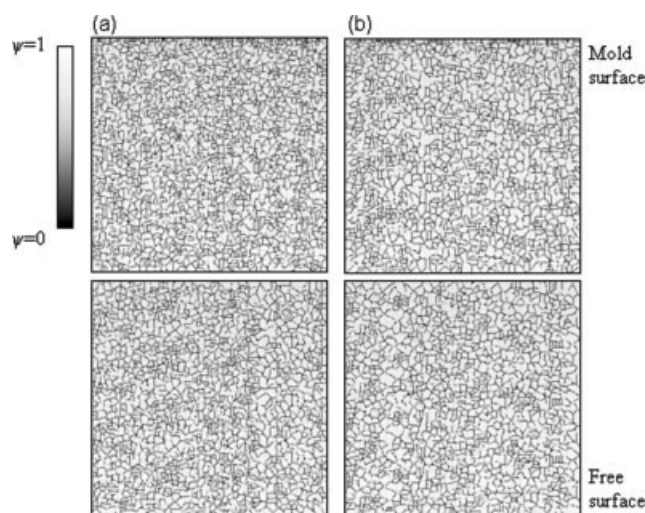

Figure 9 Simulation results showing the morphology of a 5-mm-thick cross section of ZN242 processed with (a) water-spray and (b) still-air cooling conditions.
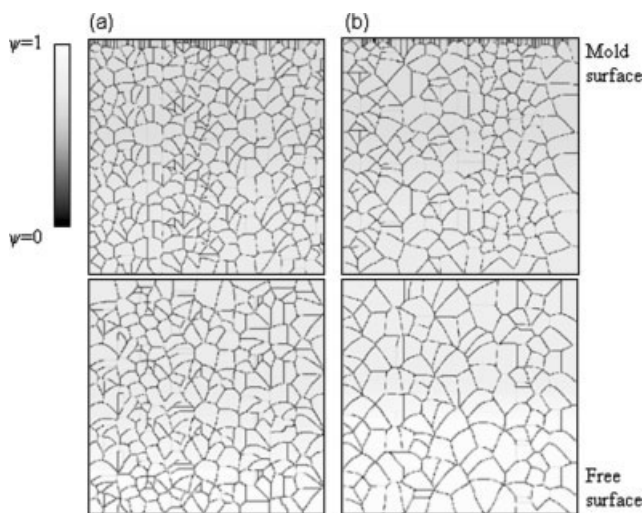
Figure 10 Simulation results showing the morphology of a 5-mm-thick cross section of S539 processed with (a) water-spray and (b) still-air cooling conditions.

only morphological features predicted at the end of the cooling stage. The results demonstrate the effect that cooling conditions have on the nature of the spherulitic growth and subsequent morphology. With the water-spray cooling method, the crystallization time at higher temperatures is shortened, favoring a higher nucleation rate and inhibiting the diffusion of polymer chain movement. The simulated picture displays finer spherulitic structures. At lower cooling rates (still-air cooling), diffusion was facilitated, and multiple nucleations were inhibited; this led to more perfect lamellae and hence higher crystallinity.

If one closely examines the morphology features of high-density copolymers (ZN242 and S244), they show a high nucleation density resulting in fine structures. This is due to the fact that as the branch content increases, the lamellae in the superstructures become shorter and then segmented, and they eventually deteriorate into small crystallites. Our model predictions also suggest that single-site-catalyst resins tend to develop larger superstructures (Figs. 10 and 11) compared with those obtained with Ziegler–Natta resins (Figs. 7–9). This is consistent with the experimental observations. Basically, the polymer resins are heterogeneous materials, and the heterogeneity may be exhibited through a distribution of differing chain lengths, differences in the chemical composition from chain to chain, or variations in the architecture of the chains as in branched and cross-linked structures. In essence, a wide range of densities of resins could be attributed to their differing branching levels. In the model calculations of the crystallization process, the influence of such heterogeneities was simulated by the incorporation of pri-

mary nucleation of polycrystalline centers. These could be represented by various critical thermal fluctuations, the amplitudes of which were determined by their own nucleation energy barriers. The supplemented small Langevin noises make these critical fluctuations either grow or dissolve.[34–36] In eq. (10), the amplitude-controlling parameter k_BT was selected to be 0.001 for single-site resins and 0.0015 for Ziegler–Natta resins. Our results suggest that the extent of heterogeneities in the molecular structure dominates the level of branching in the selection of parameters for the crystallization kinetics (nucleation rate and crystal growth velocities).

Our modeling captured the general morphology patterns with the length scale of spherulites in the Ziegler–Natta resins as well as the single-site resins. However, the experimental observations showed details of the regions, with small spherulites streaming among structures with a larger scale (Figs. 2, 3, and 5), something that did not appear in the simulation pictures. Such a phenomenon is expected for Ziegler–Natta copolymers because of the variability in their molecular structure, but it was also observed for single-site resins (Fig. 5). These morphological features, combined with the CDBI values (Table I), suggest that the single-site resins have a certain level of heterogeneity in their molecular structure in comparison with conventional metallocene resins. Intramolecular homogeneity with intermolecular heterogeneities in the comonomer distribution could have been obtained through the use of combined catalysts and/or multiple-reactor technologies. A model based on material properties represents an average for the material and does not distinguish between populations of molecules having different molecular structures. Deviations between model predictions and Ziegler–
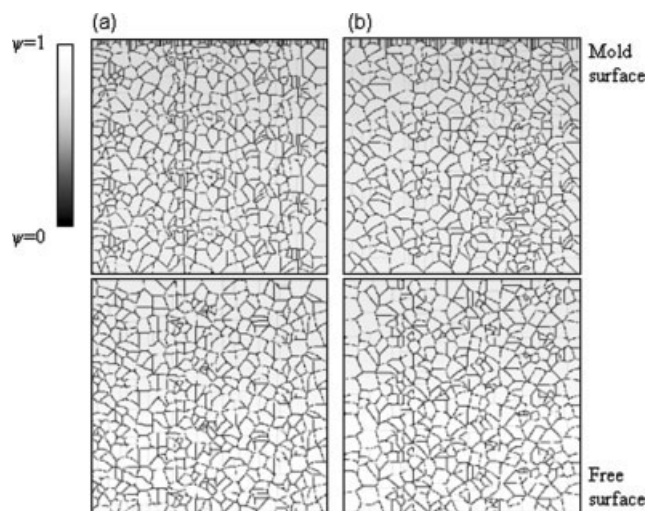

Figure 11 Simulation results showing the morphology of a 5-mm-thick cross section of S244 processed with (a) water-spray and (b) still-air cooling conditions.

Natta resins are thus expected, given the dispersity in the comonomer distribution among molecules.

CONCLUSIONS

In this article, we have demonstrated that the modified phase-field model is capable of capturing spatio-temporal morphology development with single-site catalysts or Ziegler–Natta catalyst resins in the rotational-molding process by accounting for the metastability of polymer crystallization. Experimental observation shows that the cooling condition plays an important role in the crystallization process. A structure gradient has been observed inside the part because of asymmetrical cooling conditions. Under slow air cooling, polymer chains have longer relaxation times at higher temperatures, and this results in spherulitic superstructures. With a more uniform short-chain branch distribution, the single-site copolymers developed well-defined spherulitic structures. The Ziegler–Natta catalyst resins were characterized by a higher nuclei density and nucleation rate and produced finer structures in their molded parts. The two-dimensional simulation predictions showed striking similarities with results observed experimentally.

The experimental and simulation results underline the differences in the crystallization kinetics between single-site and Ziegler–Natta catalyst resins. With higher short-chain branching content and heterogeneity in Ziegler–Natta resins, the free-energy barrier to nucleation was lower, and the chain segment had higher mobility, which enabled fast diffusion toward the crystal growth front. Thus, it developed a higher nuclei density and a higher crystallization rate, and the crystallization temperature correspondingly decreased. As a result, it produced smaller, imperfect crystals with a lower degree of crystallinity. We evaluated the influence of the molecular structure (catalyst system) on the solidification behavior in rotational molding. A direct relationship, however, cannot be established without the consideration of densification phenomena as well as degradation reactions, the latter being influenced not only by the molecular structure but also by the material formulation (additives and catalyst residues).

The modeling approach proposed in our work is new and captures both processing and material effects on the development of morphological features during melt solidification. Most model parameters can be easily determined experimentally, and simulation results provide quantitative information about the stability of the crystalline structure formed across the molded part. This last aspect is an important advance in this field of study, morphological features being important contributing factors to product performance in rotational molding.

References

1. Wang, X.; Harkin-Jones, E. H.; Crawford, R. J.; Fatnes, A.-M. Plast Rubber Compos 2000, 29, 340.
2. Annechini, D.; Takács, E.; Vlachopoulos, J. Proc Soc Plast Eng Annu Tech Conf 2001; Vol. 1; p 1291.
3. Maziers, E. Proc Soc Plast Eng Annu Tech Conf 2001; Vol. 1.
4. Wang, W.; Kontopoulou, M. Polym Eng Sci 2004, 44, 496.
5. Hay, H.; Weber, M.; Donaldson, R.; Gibbons, I.; Bellehumeur, C. Proc Soc Plast Eng Annu Tech Conf 2004; Vol. 1, p 865.
6. Pick, L. T.; Harkin-Jones, E.; Oliveira, M. J.; Cramez, M. C. J Appl Polym Sci 2006, 101, 1963.
7. Xu, H.; Bellehumeur, C. T. J Appl Polym Sci 2006, 102, 5903.
8. Wild, L.; Ryle, T. R.; Knobeloch, D. C.; Peat, I. R. J Polym Sci Polym Phys Ed 1982, 20, 441.
9. Hoffman, J. D.; Weeks, J. J. J Res Natl Bur Stand Sect A 1962, 66, 13.
10. Throne, J. L. Polym Eng Sci 1972, 12, 335.
11. Crawford, R. J.; Nugent, P. J. Plast Rubber Process Appl 1989, 11, 107.
12. Gogos, G.; Olson, L. G.; Liu, X.; Pasham, V. R. Polym Eng Sci 1998, 38, 1387.
13. Xu, L.; Crawford, R. J. Plast Rubber Compos Process Appl 1994, 21, 257.
14. Greco, A.; Maffezzoli, A.; Vlachopoulos, J. Adv Polym Technol 2003, 22, 271.
15. Martin, J. A.; Cramez, M. C.; Oliveira, M. J.; Crawford, R. J. Macromol Sci Phys 2003, 42, 367.
16. Xu, H.; Matkar, R.; Kyu, T. Phys Rev E 2005, 72, 011804.
17. Xu, H.; Keawwattana, W.; Kyu, T. J Chem Phys 2005, 123, 124908.
18. Xu, H.; Chiu, H. W.; Okabe, Y.; Kyu, T. Phys Rev E 2006, 74, 011801.
19. Caginalp, G.; Fife, P. C. Phys Rev B 1986, 33, 7792.
20. Caginalp, G. Phys Rev A 1989, 39, 5887.
21. Kobayashi, R. Phys D 1993, 63, 410.
22. Wheeler, A. A.; Boettinger, W. J.; Mcfadden, G. B. Phys Rev A 1992, 45, 7424.
23. Kyu, T.; Mehta, R.; Chiu, H.-W. Phys Rev E 2000, 61, 4161.
24. Grier, D.; Ben-Jacob, E.; Clarke, R.; Sander, L. M. Phys Rev Lett 1986, 56, 1264.
25. Sawada, Y.; Dougherty, A.; Gollub, J. P. Phys Rev Lett 1986, 56, 1260.
26. Hohenberg, P. C.; Halperin, B. I. Rev Mod Phys 1977, 49, 435.
27. Elder, K. R.; Drolet, F.; Kosterlitz, J. M.; Grant, M. Phys Rev Lett 1994, 72, 677.
28. Allen, S.; Cahn, J. W. Acta Metall 1979, 27, 1085.
29. Chiu, F. C.; Peng, Y.; Fu, Q. J Polym Res 2002, 9, 175.
30. Hsieh, E.; Fu, Q.; Cheng, S. Z. D. J Macromol Sci Phys 1997, 36, 568.
31. Bensason, S.; Minick, J.; Moet, A.; Chum, S.; Hiltner, A.; Baer, E. J Polym Sci Part B: Polym Phys 1996, 34, 1301.
32. Alfonso, G. C.; Ziabicki, A. Colloid Polym Sci 1995, 273, 317.
33. Alamo, R. G.; Blanco, J. A.; Agarwal, P. K.; Randall, J. C. Macromolecules 2003, 36, 1559.
34. Granasy, L.; Borzsonyi, T.; Pusztai, T. Phys Rev Lett 2002, 88, 206165.
35. Granasy, L.; Pusztai, T.; Warren, J. A. J Phys: Condens Matter 2004, 16, R1205.
36. Castro, M. Phys Rev B 2003, 67, 035412.
37. Rao, M. A.; Throne, J. L. Polym Eng Sci 1972, 12, 237.
38. Hoffman, J. D.; Davis, G. T.; Lauritzen, J. I., Jr. In Treatise on Solid State Chemistry; Hannay, N. B., Ed.; Plenum: New York, 1976; Chapter 7, p 479.